ACS APPLIED MATERIALS & INTERFACES

Research Article

www.acsami.org

Surface Patterning of Mesoporous Niobium Oxide Films for Solar Energy Conversion

Myoung-Ryul Ok,[†,‡] Rudresh Ghosh,[§] M. Kyle Brennaman,[‡] Rene Lopez,[†,§] Thomas J. Meyer,[‡] and Edward T. Samulski*[,‡]

[†]Curriculum in Applied Sciences and Engineering, [‡]Department of Chemistry, and [§]Department of Physics and Astronomy, University of North Carolina at Chapel Hill, CB 3290, North Carolina 27599-3290, United States

ABSTRACT: An array of periodic surface features were patterned on mesoporous niobium oxide films by a soft-lithographic technique with the goal of constructing a photonic crystal (PC) structure on the back side of the oxide. The oxide films, fabricated by mixing sol–gel derived niobium oxide nanoparticles and hydroxypropyl cellulose, were employed as photoelectrodes in dye-sensitized solar cells (DSSCs), and their performance evaluated against their flat counterparts. The surface patterns were imprinted using a photocurable perfluoropolyether (PFPE) soft-replica of a silicon master with a two-dimensional array of cylindrical posts (200 nm (D) × 200 nm (H)) in hexagonal geometry. The PC on the niobium oxide surface caused large changes in optical measurements, particularly in the blue wavelengths. To evaluate the optical effect on solar energy conversion, the incident photon-to-current conversion efficiency (IPCE) was measured in the patterned devices and the control group. The IPCE of patterned niobium oxide anodes exhibited a relative enhancement in photocurrent generation over the wavelength range corresponding to the higher absorption in optical measurements.

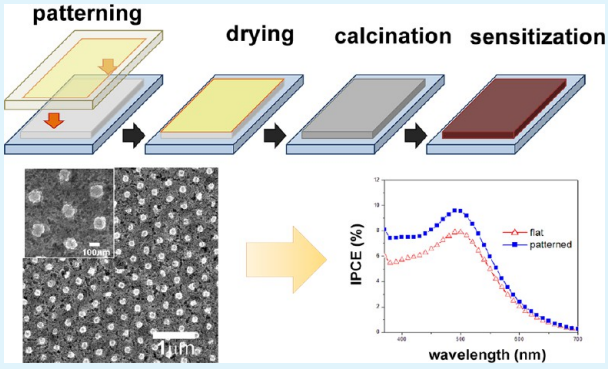

KEYWORDS: *niobium oxide, surface patterning, soft-lithography, photonic crystal, dye-sensitized solar cell*

INTRODUCTION

Since the first report of a high efficiency (~7.1%) dye sensitized solar cell (DSSC) by O'Regan and Grätzel,[1] the DSSC has been promoted as a promising photovoltaic technology with lower intrinsic costs compared to conventional Si-based photovoltaic devices. Subsequently, extensive and intensive research has focused on improving DSSC efficiency, mainly by the development of new dye molecules absorbing over a wider spectrum of light,[2,3] novel electrolytes,[4−6] the design and optimization of cell nanostructures (e.g., tubular[7,8] or nanoforests[9] of TiO_2), and new metal oxides and/or doped materials in addition to titania for dye supports.[10−13] Niobium oxide has been a candidate in those efforts to replace TiO_2, especially noteworthy for its higher conduction band energy,[11,14−17] which can be a benefit in principle by generating a higher open circuit voltage.[18] Recently, a high conversion efficiency (4.1%) cell having only a 4 μm thick Nb_2O_5 nanoporous network was reported.[19] Another application of niobium oxide with its higher conduction band energy is a shell material of the TiO_2/Nb_2O_5 core/shell structured DSSCs, forming an energy barrier to lower the recombination loss.[20,21] Along with the efforts to apply niobium oxide to DSSCs and produce photocurrents, other approaches are underway to use niobium oxide as the wide band gap semiconductor electrode for solar fuel production, for example, hydrogen generation with the dye-sensitized photoelectrochemical cells (DSPECs).[22] An additional variable to exploit to obtain better performance with existing materials is to utilize optical structures within the DSSCs for improving photon absorption and photocurrent generation.[23−31] These optical elements have been utilized extensively in TiO_2 based DSSCs. Utilizing for instance additional layer of larger TiO_2 particles for effective scattering that confines light in the dye-sensitized mesoporous TiO_2 layer,[23] or including a photonic crystal (PC) layer on top of the conventional mesoporous TiO_2 film for forming a photonic stop band and reflecting unabsorbed photons back to the mesoporous TiO_2 layer.[24−31] In some particularly effective cases, three-dimensional (3-D) opal-like structures formed with monodisperse polystyrene (PS) beads were employed to create the photonic crystal layer.[24−30] This structure is advantageous because one can easily choose the photonic stop band wavelength by simply selecting the diameter of the PS beads, especially targeting the red region where intrinsic photon absorption by the dye molecules is weak.[29] However, despite the benefits of the inverse opal based bilayer structures, its construction is a complex multistep processes, limiting the practical application of PC structures to the DSSCs. Actual enhancements in cell efficiency with good reproducibility are

Received: February 15, 2013
Accepted: March 27, 2013
Published: March 27, 2013

dx.doi.org/10.1021/am400598u | ACS Appl. Mater. Interfaces 2013, 5, 3469−3474

rare.[30] Although two-dimensional (2-D) PC structures are not as effective as the 3-D PCs which form a complete photonic band gap (PBG),[32] 2-D PCs in the form of surface patterning by soft-lithography[33] can be an alternative approach, considering the easy and simple methods to fabricate them, and 2-D PCs have been applied to organic photovoltaic devices[34] and solid state DSSCs.[35]

Herein, we describe a simple surface patterning method based on the soft-lithographic techniques to form PC structures on the nanocrystalline niobium oxide film surface. A photocurable perfluoropolyether (PFPE)[36,37] was used to replicate 2-D patterns on a Si master and reproduce them on the surface of mesoporous niobium oxide anodes; the method exploits the low surface energy and high gas permeability of PFPE.[38] Optical characteristics and solar energy conversion performances of the surface patterned niobium oxide films were analyzed and compared to flat niobium oxide anodes.

EXPERIMENTAL SECTION

Mesoporous nanocrystalline niobium oxide films were prepared on FTO coated glass substrates via a sol–gel route. A volume of 1.255 mL (0.005 mol) of niobium ethoxide ($Nb(OEt)_5$, 99.95%, Aldrich) was dissolved in 10 mL of ethanol, and 1 mL of this mixture was hydrolyzed with 0.3 mL of ammonium hydroxide solution (29.53%, Fisher Scientific). After hydrolysis, 1 mL of glacial acetic acid (99.9%, Fisher Scientific) was added to the hydrolyzed mixture, sonicated, and stirred overnight for peptization. To this niobium oxide mixture, 1.7 mL of hydroxypropyl cellulose (M_w = 100 000, Aldrich) solution in deionized water (10 wt %) was added and well mixed by stirring overnight. The as-prepared paste was used for mesoporous niobium oxide base layer, and condensed paste was used for additional surface patterning on top of the base layer. FTO coated glass substrates (15 Ω/sq, 2.3 mm thick, Hartford glass) were sonicated in acetone (99.5%, Fisher Scientific), isopropanol (99.9%, Fisher Scientific), and deionized water for 20 min each and then heat-treated at 500 °C in the air for 10 min to completely remove organic residues before coating the niobium oxide paste. Niobium oxide paste was dropped onto FTO coated glass substrate districted by the tape spacers (3M), dried on a hot plate (80 °C), and then calcined in a tube furnace to 600 °C (2 K/min) with mild air stream.

For surface patterning on top of the calcined niobium oxide films by soft-lithography, patterned polymeric mold was prepared by following the method reported by Hampton et al.:[39] Photocurable PFPE solution (a solution consisting of 1000 g/mol PFPE α,Ω-functionalized dimethacrylate and 2,2-diethoxyacetophenone as the photoinitiator) was poured and spread evenly onto a patterned Si-wafer. The surface pattern used was an arbitrarily chosen two-dimensional hexagonal array of cylindrical posts (200 nm (D) × 200 nm (H)) with 400 nm periodicity which was anticipated to exhibit observable effects in the visible wavelength range. After purging with N_2 gas for 3 min, PFPE was polymerized on a Si patterns by radiating UV light for 3 min. The photocured PFPE film was carefully removed from the Si master and rinsed with ethanol to remove uncross-linked residues on the PFPE film. Si wafer grade flat PFPE films were also made by using a nonpatterned, flat Si wafer for preparing nonpatterned niobium oxide anodes as a control. Scheme 1 summarizes the steps for fabricating surface patterned niobium oxide films: On top of these flat and patterned PFPE films, a very small amount of condensed niobium oxide paste was spread evenly. Then, the PFPE molds with very thin paste layer were put onto the calcined niobium oxide layer (Scheme 1a, b). Mild pressure was exerted to the calcined layer/additional paste layer/PFPE-mold assembly to ensure good mechanical contact among them during the drying step (in an 80 °C oven). After sufficient drying, additional niobium oxide paste layer (dried, patterned, or flat) and the calcined niobium oxide film got fused into a single solid entity (Scheme 1c). Then, the niobium oxide films with additional dried layer were calcined again in the tube furnace to 600 °C (2 K/min) with sufficient air stream.

Scheme 1. Procedure for Forming Mesoporous Patterned Niobium Oxide Film Using a Photocured PFPE Mold

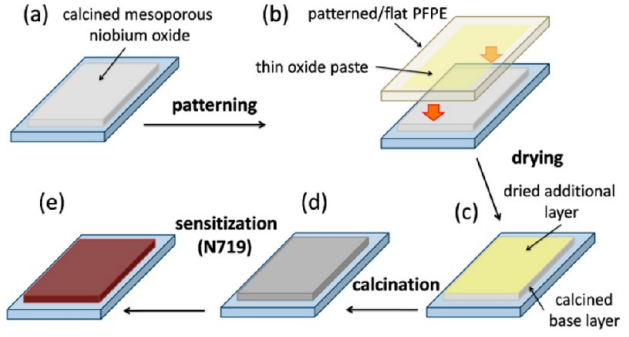

Crystallographic characterization was performed with X-ray diffraction (Rigaku MultiFlex X-ray diffractometer, Cu Kα radiation, 40 kV-40 mA, scan speed 4°/min) and a tunneling electron microscope (TEM, 100-CX, JEOL). Morphological information of the calcined niobium oxide films and surface patterns was obtained with a scanning electron microscope (SEM, S-4700, Hitachi). UV–visible absorption spectra were collected with an integration sphere (Cary 5000 fitted with DRA 2500). A surface profilometer (KLA Tencor *P*-6, scan speed = 50 μm/s, scan length = 5 mm) was used to measure the thickness of prepared films.

To evaluate the solar energy conversion performance of flat and patterned niobium oxide films, prepared films were sensitized with N719 dye and assembled to DSSCs: N719 dye was dissolved to a 1:1 mixture of acetonitrile and *t*-butanol (0.2 mM), and the solution was then centrifuged to remove aggregates. Before sensitization, prepared niobium oxide films were heat treated (500 °C for 30 min) and cooled down to 80 °C, and carefully submerged into the N719 dye solution. The films were sensitized overnight in the solution and then rinsed with acetonenitrile to wash off unabsorbed portion of dye. The sensitized niobium oxide films were shaped to ∼5 mm × 5 mm with a razor blade. Sealed DSSCs were prepared basically following methods in the literature,[40] using a 100 μm Surlyn spacer and drilling one hole for electrolyte injection. The redox electrolyte used was a solution of 0.5 M LiI and 0.05 M I_2 in dry acetonitrile. A 75 W Xe Oriel 6251/Oriel Cornerstone 260 monochromator coupled with a Keithley 6517A current meter was used to measure the incident photon-to-current conversion efficiency (IPCE).

RESULTS AND DISCUSSION

The surface images of the calcined niobium oxide samples are shown in Figure 1. Patterns were well developed maintaining their original periodicity, 400 nm, as shown in Figure 1a. One can see that the diameter of the individual features is much smaller than 200 nm, the original diameter of the cylindrical posts on the Si master. As the patterns were made of a paste containing oxide nanoparticles and a polymeric additive, a large amount of shrinkage occurs during the calcinations by the removal of the residual solvent and polymeric phase and interconnection between oxide nanoparticles. However, even with the change in detailed shape of individual features relative to the original mold, the resulting surface structures exhibited the periodic 2-D spatial dimensions which constitute a PC geometry. The surface of the niobium oxide film revealed a mesoporous fine structure of around 10 nm (based on the smallest dimension) particles, as shown in Figure 1b. Note that the top surface shows only the nanostructures of an additional layer formed by patterning; that layer experienced the calcination process just once, whereas the bulk of the niobium oxide base layer was calcined twice. In Figure 1c, one can clearly see the bilayer structure through a defective top layer.

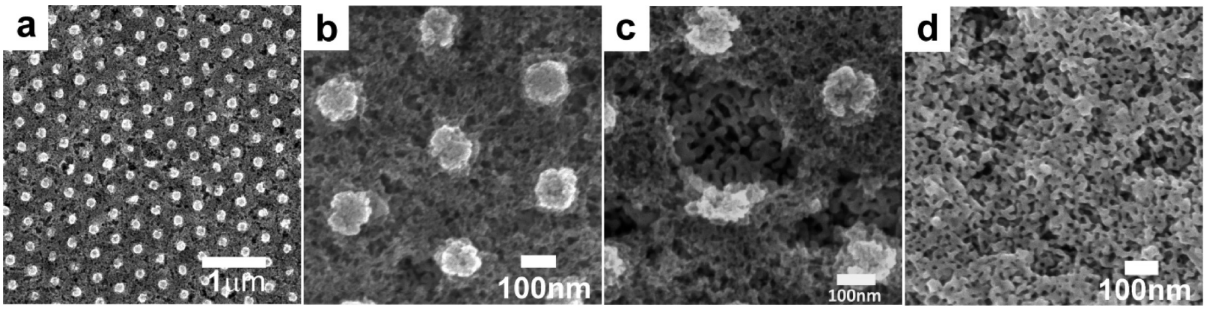

Figure 1. SEM images of the patterned niobium oxide films in different magnifications (a–c) exhibiting mesoporous surface morphology. The bilayer structure of the thin top layer on a coarser base layer is evident through a surface defect in the top layer in (c), and the morphology of the base layer achieved by calcining a film twice is shown in (d).

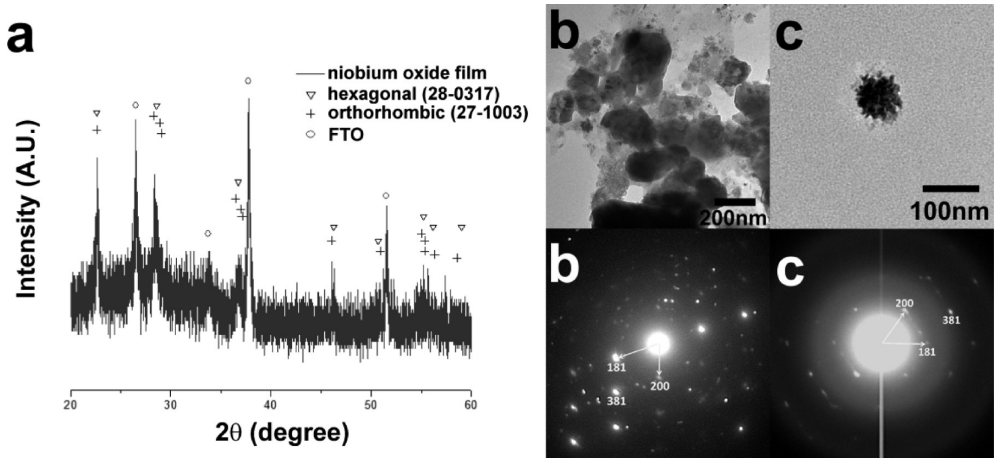

Figure 2. Crystallographic analysis of the prepared niobium oxide by using (a) XRD and (b, c) TEM. SAED patterns in (b) and (c) revealed an orthorhombic crystal structure with a zone axis $[01\bar{8}]$.

The dimensions of the base layer were much coarser than the top layer. To resolve the morphological discrepancy between the fine top layer and the coarse base layer, a monolayer with equivalent thermal history to the base layer (double calcinations with heating rate of 2 K/min to 600 °C) was prepared and observed with an SEM. As shown in Figure 1d, a layer with double calcination steps exhibited a bicontinuous mesoporous structure with coarser particle size about 20–40 nm, which matches well to the image of the base layer exposed in Figure 1c. The particles were so well connected that one cannot discriminate individual nanoparticles from each other in the SEM images. This implies that the morphology of the base layer would have been like the fine structure of the top layer surface shown in Figure 1b after the first calcination, and then became coarse and bicontinuous by the second calcination step. In terms of solar energy conversion, this coarser but bicontinuous nanostructure could be beneficial in electron transport, while detrimental to dye loading, in general.

Crystallographic information of the niobium oxide films were analyzed with X-ray diffraction (XRD) and transmission electron microscopy (TEM). In Figure 2a, XRD data are shown. Considering the process conditions and resultant crystal structure in the literature,[22,41] it appears that the crystal structure of the prepared niobium oxide film is orthorhombic structure (JCPDS #27-1003). However, as shown in Figure 2a, most of the main peaks of both an orthorhombic and a hexagonal structure (JCPDS #28-0317) are so close that it is very difficult to identify one from the other solely by XRD from a thin film on a substrate. So, TEM was used to collect more crystallographic evidence. Figure 2b and c shows TEM images of the niobium oxide particles and selected area electron diffraction (SAED) pattern of them prepared by grinding the niobium oxide film. The TEM image in Figure 2b exhibited fragmented nanoparticles and larger globular structures together. Though the globular structures are an order of magnitude larger than the average particle size of the coarse base layer, they revealed many sections in contrast and looked like overlapped particles of several tens of nanometers. So, considering the SEM images shown in Figure 1, they are believed to be the globular flakes of the prepared oxide film which were the interconnected structure of the nanocrystalline niobium oxide particles. From the SAED pattern in Figure 2b, the crystal structure of the niobium oxide nanoparticles was identified as orthorhombic structure (T-phase) with a zone axis $[01\bar{8}]$. This matches well with the crystal structure and process conditions reported in the literature.[20,39] However, there exists discrepancy in the thermal history of the top and base layers, and the top layer is the most probable position where the residual low temperature hexagonal phase could exist. Figure 2c shows the TEM image of the small ground structure and SAED pattern from it. Considering the size of the nanoparticles in it, it is evident that the particle is a part of the top layer fired once. The SAED pattern in Figure 2c was also identified as the orthorhombic structure with the same zone axis $[01\bar{8}]$. So, it can be concluded that both top and base layers consist of nanocrystalline orthorhombic niobium oxide particles.

The optical properties of the flat and patterned niobium oxide films were measured in the UV–visible range. Initially,

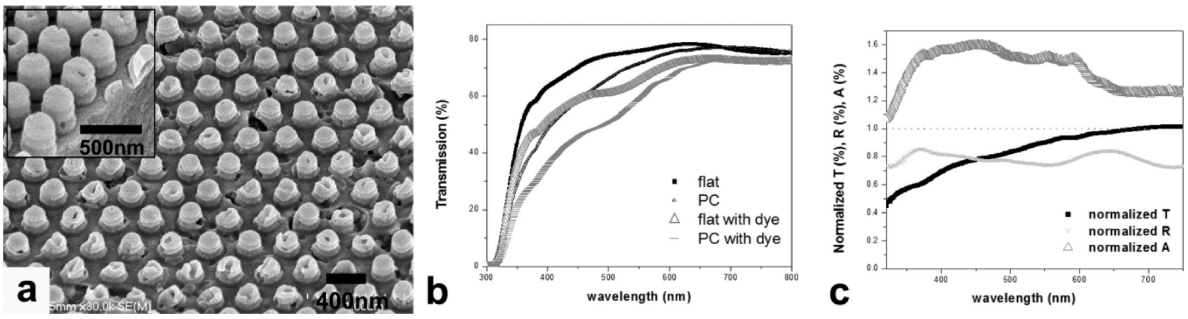

Figure 3. (a) SEM image of the dense patterns made of an oxide paste without polymeric additives. (b) Transmission spectra of flat and patterned niobium oxide films with and without dye loading. (c) Normalized transmission, reflection, and absorption spectra from a patterned film relative to a flat film as a function of wavelength.

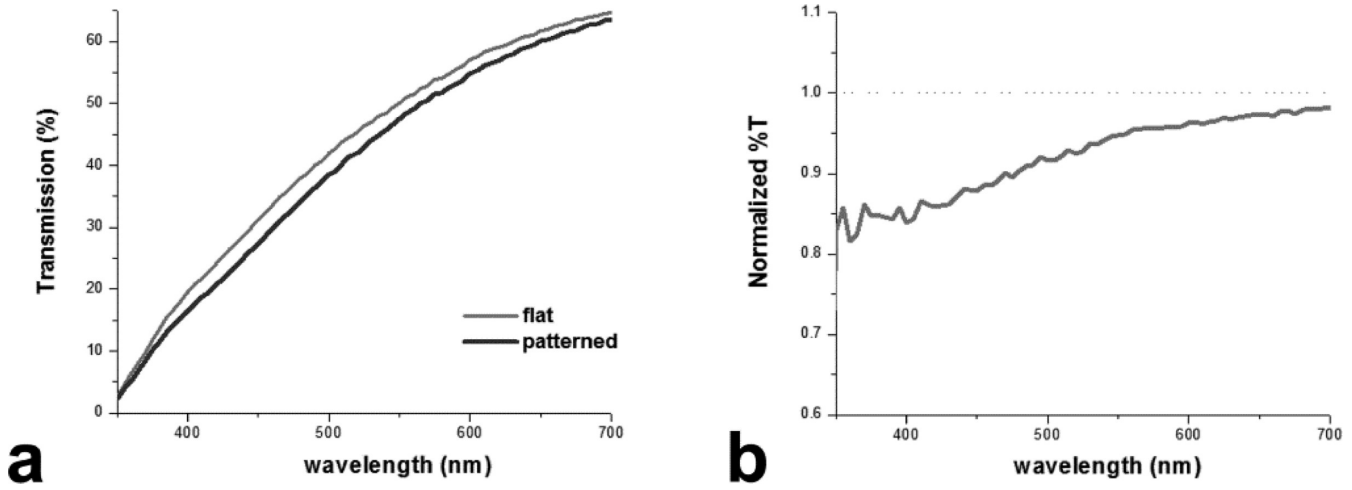

Figure 4. (a) Transmission spectra of flat and patterned films with mesoporous top layers. (b) Normalized transmission of the PC sample relative to the flat film.

apart from the mesoporous niobium oxide films shown in Figure 1, denser surface patterns were produced (by not adding polymeric additives to the oxide paste) to maximize the photonic crystal effect: when making photonic crystal structures, selection of two materials with high refractive index contrast yields the most effective effect.[32] In our surface patterning study, one material of the repeating unit is either air (refractive index = 1), in optical measurements, or the redox electrolytes in actual solar energy conversion experiments, for example, acetonenitrile (n = 1.34) in DSSCs; the other material is the niobium oxide (refractive index = 2.39[42]). Once the intrinsic refractive index of two materials for patterning is determined, maximization of refractive index difference could be achieved by forming dense niobium oxide patterns: porous materials have refractive index between the neat materials and the air filling the pores.

SEM images of the dense surface patterns are shown in Figure 3a, and the transmission spectra in the UV−visible range of flat and patterned niobium oxide film with and without dyes are shown in Figure 3b. One can see a clear decrease in transmission by the surface patterned films, especially in the blue range, both with and without dye loading. The net change of transmission, reflection, and absorption by patterning are illustrated in Figure 3c by normalizing the spectra from the patterned niobium oxide film to those from flat films. It can be seen from the plot that the effect of patterning on the optical property is distinct over a wide wavelength range. Moreover, PC effect is evident especially in the normalized transmission and absorption spectra, despite the large degree of variation with wavelength and the relatively small variation of normalized reflection spectra with wavelength. Indeed, it was confirmed from Figure 3b and c that the dense surface patterns on the surface constituted a PC structure strongly interacting with UV and visible light. However, the niobium oxide paste used to build dense patterns had critical problems in the surface patterning steps: as the paste did not contain polymeric additives, the additional layer dried too quickly when spread onto patterned PFPE mold and it could not be fused to the base layer. So, it was really hard to pattern a large area uniformly. Also, when spread onto the base layer and covered with a patterned mold to avoid the "quick drying" problem, as the viscosity of the oxide paste without a polymeric additive is too small, it flows into the pores in the base layer and makes it less porous, rather than staying within the space between mold and base layer for patterning. Consequentially it was essential to stabilize the fabrication processes by using an oxide paste containing a polymeric additive while sacrificing some portion of the benefit of dense patterns; it would be meaningful to compare the optical properties of PCs made from porous patterns to those made from dense oxide patterns.

Optical transmission spectra of mesoporous top layers (flat and/or patterned) identical to the films shown in Figure 1 are shown in Figure 4a. Although not so distinct as in the spectra of dense patterns, a drop in the transmitted intensity can be seen in the raw spectra. The normalized transmission in Figure 4b indicates that the mesoporous patterns also formed a PC

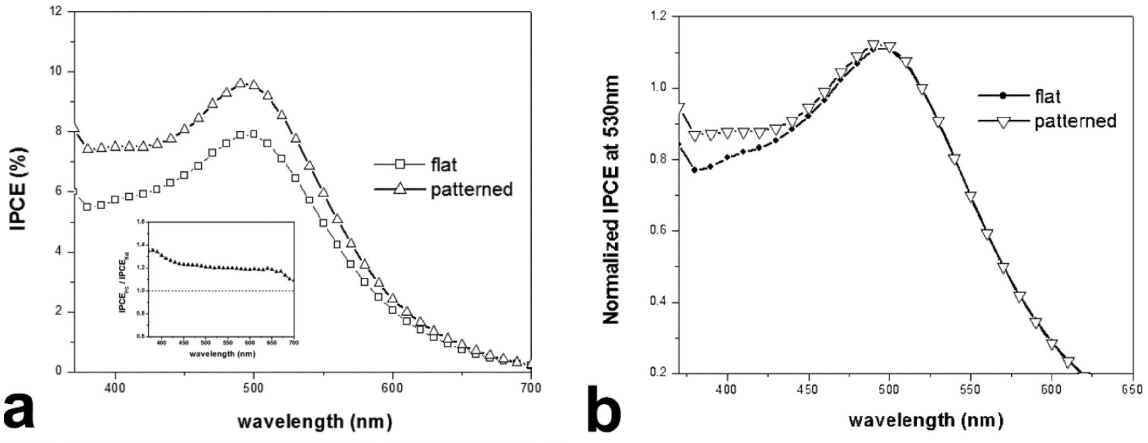

Figure 5. IPCE of flat and PC samples. Inset in (a) shows the normalized IPCE of a PC sample relative to a flat sample; (b) the normalized IPCE of flat and PC samples at 530 nm, revealing an enhancement of IPCE in the blue range.

structure exhibiting decrement in transmission close to 20% around the 400 nm wavelength range. Although the decrement of the normalized transmission by the mesoporous patterns was about a half of the value exhibited by dense patterns, considering the huge benefits of the polymer-containing oxide paste in the fabrication processes, the degradation of PC performance with mesoporous patterns is acceptable.

In order to observe how the optical effects by the superficial PC structure can actually affect the photocurrent generation, the flat and patterned niobium oxide electrodes were prepared in sealed DSSCs and the incident photon-to-current conversion efficiency (IPCE) was measured. Figure 5a is the IPCE of flat and patterned samples versus wavelength. The patterned sample exhibited higher IPCE values than the flat sample over the whole wavelength range shown. This is emphasized in the inset, which is the normalized IPCE of the sample with PC to the IPCE of a flat reference sample. The normalized IPCE curve in the inset lies above one, meaning that all IPCE values of the PC structure were greater than the IPCE of the flat sample. Although the patterned sample was 3.6% thicker than the flat sample (2.971 and 2.864 μm, respectively), normalized IPCE revealed a much larger difference which could not to be explained by the thickness difference. To clarify the PC effect as a function of wavelength, the IPCE of the each sample was normalized at 530 nm, as shown in the Figure 5b. It is notable that the increment in IPCE exhibited by the PC structure becomes more distinct as the wavelength of the photons decreases, which is in good agreement with the trend observed in the optical measurements in Figure 4b. This implies that the decrement of light transmission by the surface PC structure could be related to the increment of the absorption of photons as confirmed in Figure 3c, and that the increased absorption of photons caused a greater generation of photocurrent. So, it can be concluded that building PC structures by merely patterning the surface is a simple but powerful strategy for enhancing light harvesting and solar energy conversion. It can be seen from the plots in Figure 5 that the surface patterns were especially more effective in the blue relative to the red end of the visible spectrum. As the patterns form a 2-D surface PC structure with an incomplete photonic band gap (PBG) rather than a 3-D structure forming a complete PBG in a narrow wavelength range,[32] it reflects photons over a wide energy span back to the mesoporous sensitized layer.[30,35] So, the blue enhancement can be explained by the combination of the two effects: On the one hand, it can be attributable to the geometry (especially the periodicity[35]) of the surface patterns used in this investigation, and one can expect different optical responses by tuning the period of the patterns. On the other hand, it is impacted by scattering in the blue wavelength region, that is, by Rayleigh scattering[30,43] as photons of higher energy scatter more in the media. So, when unabsorbed photons are reflected back to the sensitized layer by the surface PC structure, reflected photons of shorter wavelength tend to have more chance for absorption. Thus, the enhancement of photon-to-current conversion by the surface patterns should increase by decreasing the wavelength of the photons, as shown in Figure 5.

Indeed, the superficial surface patterns described here are quite an effective strategy to incorporate PC effects into DSSC devices using a much simpler fabrication process relative to 3-D photonic crystal structures. In addition, as the PC effects result from combinations of refractive indices of materials and geometry of the patterns,[32] if we apply the same patterns used in this study to other oxide semiconductor materials with similar refractive index, we can expect similar enhancement in solar energy conversion. Moreover, the hexagonal array of cylindrical posts investigated in this study was selected from extant patterns, not designed intentionally for optimal effects. This implies that more enhancements of IPCE than reported in this study are likely to be achieved by optimization of the geometry of the surface patterns.

CONCLUSIONS

A simple surface patterning technique using a photocurable PFPE was applied to form photonic crystal structures on the mesoporous niobium oxide films. The surface patterns were well replicated using a PFPE mold on top of a preformed base layer with minimal changes in the dimensions of the oxide morphology. Even though surface structures exhibited changes in the detailed shape and dimensions relative to that of the mold, they retained the attributes of an ordered array retaining periodicity of the mold. Synthesized niobium oxide nanoparticles in the top and base layers had an orthorhombic structure (T-phase) irrespective of the number of calcination steps. Optical measurements showed that the surface patterns formed a PC structure resulting in increased absorption of photons, especially in the blue wavelength region. By this surface alteration of the optical behavior of niobium oxide films, more photocurrent was generated in solar energy conversion

experiments using DSSCs. The IPCE was enhanced by the surface PC structure over the whole wavelength range of the UV−visible spectrum, but the enhancement was more distinct in the blue range, agreeing with the optical measurement. In summary, mesoporous surface patterns on niobium oxide electrodes can be readily formed into a photonic crystal structure that effectively enhances the photocurrent generation. This surface patterning strategy can also be applied to other mesoporous oxide semiconductor materials having similar refractive indices (e.g., titanium oxide and zinc oxide) routinely used in DSSCs.

AUTHOR INFORMATION

Notes

The authors declare no competing financial interest.

ACKNOWLEDGMENTS

This material is based upon work wholly supported as part of the UNC EFRC: Center for Solar Fuels, an Energy Frontier Research Center funded by the U.S. Department of Energy, Office of Science, Office of Basic Energy Sciences under Award Number DE-SC0001011. Also, authors are grateful to the instrumental support of CHANL (Chapel Hill Analytical and Nanofabrication Laboratory) for our analytical parts in this study.

REFERENCES

(1) O'Regan, B.; Grätzel, M. *Nature* **1991**, *353*, 737−740.
(2) Nazeeruddin, M. K.; Kay, I.; Rodicio, A.; Humphry-Baker, R.; Müller, E.; Liska, P.; Vlachopouloss, N.; Grätzel, M. *J. Am. Chem. Soc.* **1993**, *115*, 6382−6390.
(3) Gao, F.; Wang, Y.; Shi, D.; Zhang, J.; Wang, M.; Jing, X.; Humphry-Baker, R.; Wang, P. M.; Zakeeruddin, S.; Grätzel, M. *J. Am. Chem. Soc.* **2008**, *130*, 10720−10728.
(4) Huang, S. Y.; Schlichthörl, G.; Nozik, A. J.; Grätzel, M.; Frank, A. J. *J. Phys. Chem. B* **1997**, *101*, 2576−2582.
(5) Kopidakis, N.; Neale, N. R.; Frank, A. J. *J. Phys. Chem. B* **2006**, *110*, 12485−12489.
(6) Yella, A.; Lee, H.-W.; Tsao, H. N.; Yi, C.; Chandrian, A. K.; Nazeeruddin, M. K.; Diau, E. W.-G.; Yeh, C.-Y.; Zakeeruddin, S. M.; Grätzel, M. *Science* **2011**, *334*, 629−634.
(7) Macak, J. M.; Tsuchiya, H.; Ghicov, A.; Schmuki, P. *Electrochem. Commun.* **2005**, *7*, 1133−1137.
(8) Roy, P.; Albu, S. P.; Schmuki, P. *Electrochem. Commun.* **2010**, *12*, 949−951.
(9) Sauvage, F.; Di Fonzo, F.; Li Bassi, A.; Casari, C. S.; Russo, V.; Divitini, G.; Ducati, C.; Bottani, C. E.; Comte, P.; Graetzel, M. *Nano Lett.* **2010**, *10* (7), 2562−2567.
(10) Tennakone, K.; Kumara, G. R. R.; Kottegoda, I. R. M.; Perera, V. S. P. *Chem. Commun.* **1999**, 15−16.
(11) Sayama, K.; Suguhara, H.; Arakawa, H. *Chem. Mater.* **1998**, *10*, 3825−3832.
(12) Jose, R.; Thavasi, V.; Ramakrishna, S. *J. Am. Ceram. Soc.* **2009**, *92* (2), 289−301.
(13) Feng, X.; Shankar, K.; Paulose, M.; Grimes, C. A. *Angew. Chem., Int. Ed.* **2009**, *48* (43), 8095−8098.
(14) Lenzmann, F.; Krueger, J.; Burnside, S.; Brooks, K.; Grätzel, M.; Gal, D.; Rühle, S.; Cahen, D. *J. Phys. Chem. B* **2001**, *105*, 6347−6352.
(15) Maruska, H. P.; Ghosh, A. K. *Solar Energy* **1978**, *20*, 443−458.
(16) Scaife, D. E. *Solar Energy* **1980**, *25*, 41−54.
(17) Grimes, C. A.; Varghese, O. K.; Ranjan, S. *Light, Water, Hydrogen: The Solar Generation of Hydrogen by Water Photoelectrolysis*; Springer: New York, 2007; pp 191−255.
(18) Wurfel, U.; Peters, M.; Hinsch, A. *J. Phys. Chem. C* **2008**, *112*, 1711−1720.
(19) Ou, J. Z.; Rani, R. A.; Ham, M.-H.; Field, M. R.; Zhang, Y.; Zheng, H.; Reece, P.; Zhuiykov, S.; Sriram, S.; Bhaskaran, M.; Kaner, R. B.; Kalantar-zadeh, K. *ACS Nano* **2012**, *6*, 4045−4053.
(20) Barea, E.; Xu, X. Q.; Gonzalez-Pedro, V.; Ripolles-Sanchis, T.; Fabregat-Santiago, F.; Bisquert, J. *Energy Environ. Sci.* **2011**, *4*, 3414−3419.
(21) Kim, H.-N.; Moon, J. H. *ACS Appl. Mater. Interfaces* **2012**, *4*, 5821−5825.
(22) Luo, H.; Song, W.; Hoertz, P. G.; Hanson, K.; Ghosh, R.; Rangan, S.; Brennaman, M. K.; Concepcion, J. J.; Binstead, R. A.; Bartynski, R. A.; Lopez, R.; Meyer, T. J. *Chem. Mater.* **2013**, *25*, 122−131.
(23) Usami, A. *Chem. Phys. Lett.* **1997**, *277*, 105−108.
(24) Nishimura, S.; Abrams, N.; Lewis, B. A.; Halaoui, L. I.; Mallouk, T. E.; Benkstein, K. D.; Lagemaat, J. V. D.; Frank, A. J. *J. Am. Chem. Soc.* **2003**, *125*, 6306−6310.
(25) Halaoui, L. I.; Abrams, N. M.; Mallouk, T. E. *J. Phys. Chem. B* **2005**, *109*, 6334−6342.
(26) Mihi, A.; Míguez, H. *J. Phys. Chem. B* **2005**, *109*, 15968−15976.
(27) Mihi, A.; López-Alcaraz, F. J.; Míguez, H. *Appl. Phys. Lett.* **2006**, *88*, 193110−193113.
(28) Herman, L. A.; Yip, C. H.; Wong, C. C. *J. Nanosci. Nanotechnol.* **2010**, *10*, 4657−4662.
(29) Guldin, S.; Hüttner, S.; Kolle, M.; Welland, M. E.; Müller-Buschbaum, P.; Friend, R. H.; Steiner, U.; Tétreault, N. *Nano Lett.* **2010**, *10*, 2303−2309.
(30) Lee, S.-H. A.; Abrams, N. M.; Hoertz, P. G.; Barber, G. D.; Halaoui, L. I.; Mallouk, T. E. *J. Phys. Chem. B* **2008**, *112*, 14415−14421.
(31) Colodrero, S.; Mihi, A.; Häggman, L.; Ocaña, M.; Boschloo, G.; Hagfeldt, A.; Míguez, H. *Adv. Mater.* **2009**, *21*, 764−770.
(32) Johnson, S. G.; Joannopoulos, J. D. *Acta Mater.* **2003**, *51*, 5823−5835.
(33) Zhao, X.-M.; Xia, Y.; Whitesides, G. M. *J. Mater. Chem.* **1997**, *7*, 1069−1074.
(34) Ko, D.-H.; Tumbleston, J.; Zhang, L.; Williams, S. S.; DeSimone, J. M.; Lopez, R.; Samulski, E. T. *Nano Lett.* **2009**, *9*, 2742−2746.
(35) Kim, J.; Koh, J. K.; Kim, B.; Kim, J. H.; Kim, E. *Angew. Chem., Int. Ed.* **2012**, *51*, 6864−6869.
(36) Rolland, J. P.; Van Dam, R. M.; Schorzman, D. A.; Quake, S. R.; DeSimone, J. M. *J. Am. Chem. Soc.* **2004**, *126*, 2322−2323.
(37) Rolland, J. P.; Hagberg, E. C.; Denison, G. M.; Carter, K. R.; DeSimone, J. M. *Angew. Chem., Int. Ed.* **2004**, *43*, 5796−5799.
(38) Maynor, B. W.; LaRue, I.; Hu, Z.; Rolland, J. P.; Pandya, A.; Fu, Q.; Liu, J.; Spontak, R. J.; Sheiko, S. S.; Samulski, R. J.; Samulski, E. T.; DeSimone, J. M. *Small* **2007**, *3*, 845−849.
(39) Hampton, M. J.; Williams, S. S.; Zhou, Z.; Nunes, J.; Ko, D.-H.; Templeton, J. L.; Samulski, E. T.; DeSimone, J. M. *Adv. Mater.* **2008**, *20*, 2667−2673.
(40) Wang, Z.-S.; Kawauchi, H.; Kashima, T.; Arakawa, H. *Coord. Chem. Rev.* **2004**, *248*, 1381−1389.
(41) Lenzmann, F.; Shklover, V.; Brooks, K.; Grätzel, M. *J. Sol-Gel Sci. Technol.* **2000**, *19*, 175−180.
(42) Kukli, K.; Ritala, M.; Leskelä, M.; Lappalainen, R. *Chem. Vap. Deposition* **1998**, *4*, 29−34.
(43) Bohren, C. F.; Huffman, D. R. *Absorption and scattering of light by small particles*; John Wiley & Sons, Inc.: Weinheim, Germany, 1983.